Supporting information for:

Last century warming over the Canadian Atlantic shelves linked to weak Atlantic Meridional Overturning Circulation

Authors

B. Thibodeau[1,2]†*, C. Not[1,2]†, J. Zhu[3], A. Schmittner[4], D. Noone[4], C. Tabor[5], J. Zhang[6], Z. Liu[7]

Affiliations

[1]Department of Earth Sciences, The University of Hong Kong, Hong Kong SAR

[2]The Swire Institute of Marine Science, The University of Hong Kong, Hong Kong SAR

[3]Department of Earth and Environmental Sciences, University of Michigan, United-States of America

[4]College of Earth, Ocean, and Atmospheric Sciences, Oregon State University, United-States of America

[5]Center for Integrative Geosciences, University of Connecticut, United-States of America

[6]CCS-2 and CNLS, Los Alamos National Laboratory, Los Alamos, New Mexico, United-States of America

[7]Atmospheric Science Program, Department of Geography, The Ohio State University, United-States of America

*Correspondence to: bthib@hku.hk

† Equal contribution

Content

Text S1 to S5

Figures S1 to S6

Additional file

Full dataset (excel file)

Introduction

This file includes additional details about modeling results, sediment cores chronology and uncertainty of the proxy used as well as statistic on the results.

1. Chronostratigraphy of climate archives

The chronostratigraphy of core MD99-2220 was originally established by St-Onges et al. (2003) based on twenty benthic mollusk shells analyzed from MD99-2220 and neighbor core MD99-2221. Correlation with a box core retrieved from the same site indicated that the top 14 cm of core MD99-2220 was missing. The age model of the upper part of core MD99-2220 was established using a box-core retrieved from the same vicinity. The cross-correlation between MD99-2220 and AH00-2220 was performed based on geochemical data (St-Onge et al., 2003; Thibodeau et al., 2006; Thibodeau et al., 2010a). The chronostratigraphy of box core CR02-23 (taken at the same site) was validated using ^{210}Pb (Thibodeau et al., 2006). Here we present an updated age model for both cores using a constant-rate supply ^{210}Pb model that calculates variable sedimentation rate for each sample, which is particularly suitable for last-century cores where sedimentation rate often changes due to anthropogenic activities (Ghaleb, 2009) (Fig S4). Due to the loss of the top 14 cm of core MD99-2220, we will not use this core for high-resolution reconstruction of the last century and rather focus on core CR02-23. While the benthic foraminifera δ^{18}O values are similar for both cores and decrease toward the younger part of the core, there is an offset of about 40 years between the appearance of the lowest value in the two cores (Fig S5). This offset could be due to sediment disturbance/compression in the upper part of the piston core.

The chronostratigraphy of gorgonian coral was done using band-counting validated by radiocarbon measurement (Sherwood et al., 2011). The subsurface Labrador Sea temperature and salinity record comes from sediment core RAPiD-35-25B (Moffa-Sánchez et al., 2014). We used the original chronology, which is based on ^{210}Pb dating of the upper part of the core and seven ^{14}C dates in the older part of the core (Moffa-Sánchez et al., 2014).

2. Uncertainties of different proxies

Measurement of δ^{18}O in core MD99-2220 and CR02-23 was performed with an analytical precision better than ±0.05 ‰, which is equivalent to a precision of about 0.15-0.20°C in temperature. Instrumental measurements of Laurentian Channel bottom water temperature were carried out with a precision of ±0.01°C (Gilbert et al., 2005). Nitrogen isotopes of coral were measured with an analytical precision better than ±0.20‰ (Sherwood et al., 2011). Subsurface salinity and temperature reconstruction of the Labrador Sea have an uncertainty of ±0.8 psu and ±0.8°C (Moffa-Sánchez et al., 2014). Analytical precision for

sortable silt was estimated at 1% (±0.3 µm), while replicates-based precision was estimated at ±0.8 µm (Thornalley et al., 2018).

3. Modeling results

In response to the freshwater forcing (0.05 Sv in the UVic and 0.10 Sv in the iCESM), the upper-ocean seawater becomes fresher and lighter, increasing stratification and inhibiting deep convection in the North Atlantic (Fig S1). As a result, the AMOC strength, indicated by the maximum transport in the North Atlantic, decreases by 17% and 28% in 100 years in UVic and iCESM, respectively. The warming is a consequence of reduced northward transport in the Gulf Stream, which requires a decrease in zonal density (temperature) gradients via thermal wind balance. The models achieve this by warming west and cooling east of ~40°W. Modeling results suggest that the reorganization of gyre circulations is a direct consequence of AMOC weakening (Saba et al., 2016; Thornalley et al., 2018). The reduced northward heat transport associated with the AMOC decreases the SST in the northern North Atlantic significantly and produces a local high-pressure anomaly (Stouffer et al., 2006). The high-pressure anomaly acts to weaken the westerlies in the mid-latitude North Atlantic and the gyre circulations. Following ref 42, a budget analysis of the subsurface temperature changes in iCESM was conducted. The analysis suggests that the net subsurface warming is primarily caused by the reduced zonal component of the Gulf Stream, as the reduced meridional flow acts to cool the subsurface water (Fig S2). It is important to note that we only applied freshwater forcing at the ocean surface and kept all other boundary conditions and forcings constant, as the parent water masses did not warm during the last century (Gilbert et al., 2005). Therefore, the subsurface temperature increase is solely due to a change in the circulation. In summary, both models suggest a warming of intermediate water in the Northwestern Atlantic of 1.5–2.5°C (Fig S1) under a weakening of the AMOC by 17–28%.

The water-isotope capability of iCESM can also help to further validate that our sedimentary $\delta^{18}O$ records actually represent changes in temperature by investigating the contribution of changes in $\delta^{18}O$ of seawater. The simulated water $\delta^{18}O$ enrichment of about 0.2–0.3‰ suggests a major increase in the proportion of $\delta^{18}O$-enriched ATSW at this location, indicating a change in western North Atlantic oceanography (Fig S3). This supports previous estimates based on temperature and dissolved oxygen changes (Gilbert et al., 2005; Thibodeau et al., 2010a). The heavier modelled $\delta^{18}O$ also discards potential effect related to the injection

of freshwater in the system. This seawater $\delta^{18}O$ enrichment could influence our benthic $\delta^{18}O$ record in the opposite way than warming, which depletes the $\delta^{18}O$ recorded in carbonate. Therefore, the amplitude of our temperature reconstruction should be considered as a conservative estimation. While a sensitivity experiment conducted with iCESM (iPOP2-Trace) suggests that the $\delta^{18}O$ of carbonate at the MD99-2220 coring location might be heavier because of change in pCO_2 (Zhang et al., 2017), the effect is also opposite to the signal observed in our record.

4. Oxygen isotopes as a record for temperature

Oxygen isotopes in carbonate marine organisms vary with the temperature of calcification and the $\delta^{18}O$ value of the water mass in which they calcify (Shackleton, 1974). This counteracting effect has been previously investigated in Laurentian channel sediment cores by comparing high-resolution benthic foraminifera $\delta^{18}O$ records to instrumental temperature and salinity data (Thibodeau et al., 2010a). It was demonstrated that $\delta^{18}O$ in benthic foraminifera underestimated the actual temperature increase (i.e., creating lighter $\delta^{18}O$) because of the increased proportion of Atlantic Intermediate Slope Water (characterized by high $\delta^{18}O$) in the Laurentian Channel. Thus, our $\delta^{18}O$ records from the St. Lawrence should be considered as a conservative tool to reconstruct the Laurentian Channel bottom water temperature, as the full temperature increase is not expressed. This signal was also observed in the model results (Fig S3), which further support our hypothesis. The relatively rapid residence time (about 7 years) and the isolation of the Laurentian channel bottom water from overlying freshwater make it resilient to other potential local processes affecting $\delta^{18}O$ and thus representative of the western North Atlantic slope waters entering the channel, irrespective of the timescale (Gilbert et al., 2005). This is further illustrated by the absence of statistically different changes in temperature and salinity along the same potential density from Cabot Strait though the St. Lawrence Estuary between 1970 and 1990, highlighting the potential for these cores to reflect the condition of the water entering the channel (Gilbert et al., 2005). Because the temperature of the bottom is directly controlled by the proportion of Atlantic Intermediate Slope Water entering the Laurentian channel, the $\delta^{18}O$ in benthic foraminifera can also be considered a tracer of changes in the regional oceanography.

5. **Statistical analysis**

We investigated the similarity of the 20th century Laurentian channel bottom water instrumental temperature, $\delta^{15}N$ of corals and the AMOC index and how well $\delta^{18}O$ of core CR02-23 recorded these trends (Fig 2) using a spearman correlation (non-parametric). We did not detrend the data, as we are mostly interested in how well the $\delta^{18}O$ of core CR02-23 captures the general trend and we wanted to minimize the influence of potential lead and lag due to sample resolution, bioturbation smoothing, and variable sedimentation rates. Results suggest a high degree of similarity between CR02-23 $\delta^{18}O$ and instrumental temperature ($r = -0.76$, $p < 0.005$), CR02-23 $\delta^{18}O$ and coral $\delta^{15}N$ ($r = 0.79$, $p < 0.005$), and CR02-23 $\delta^{18}O$ and AMOC index ($r = 0.49$, $p < 0.005$). We also observed a high correlation between the AMOC index and instrumental temperature ($r = -0.8$, $p < 0.005$), dissolved oxygen ($r = 0.85$, $p < 0.005$), and the coral $\delta^{15}N$ ($r = 0.68$, $p < 0.005$). The coral $\delta^{15}N$ is also similar to the instrumental temperature ($r = -0.77$, $p < 0.005$).

The 20th century values in core MD are significantly different when comparing them to both the complete record (~700–1960), the pre-1600, and the 1600-1899 period ($p < 0.005$ for both Kruskal-Wallis and one-way ANOVA). Using the same tests, we found that the 1600-1899 period is not significantly different from the complete record, but it is significantly different from the pre-1600 record ($p < 0.05$ for both Kruskal-Wallis and one-way ANOVA). The means and the 95% confidence interval for each period can be seen in Fig S6.

Supplementary Figures

Figure 1. Modelled impact of a weakening of the AMOC on the temperature in the western North Atlantic.

Figure 2. Budget analysis of the subsurface warming.

Figure 3. Attributing response of subsurface carbonate $\delta^{18}O$ to freshwater forcing in iCESM.

Figure 4. Updated age models for core piston core MD99-2220 and its box core AH00-2220 and box core CR02-23.

Figure 5. $\delta^{18}O$ from core MD99-2220 (red) and CR02-23 (pink) and $\delta^{15}N$ from Sherwood's corals.

Figure 6. Means and confidence intervals (95%) of the different time periods in core MD99-2220
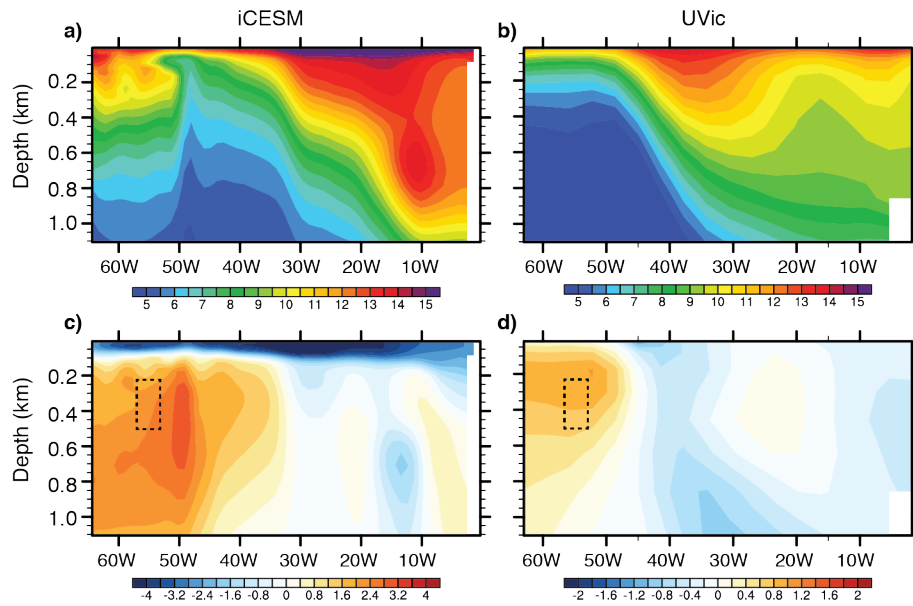
Figure S1. Modelled impact of a weakening of the AMOC on the temperature in the western North Atlantic. In the bottom panel we illustrate the modeled ocean temperature changes over the Northwest Atlantic after 100 years of freshwater forcing in the iCESM and UVic model. Depth-longitude section of ocean temperature in the upper 1,000 m of the western North Atlantic at 45°N in the preindustrial control simulation (**a,b**) and the changes after 100-year water hosing (**c,d**). We can observe the warming of the intermediate water of 2–2.5°C and 1–1.5°C next to the Laurentian channel entrance (dashed boxes) in the iCESM and UVic model, respectively. Note that the magnitude of the freshwater forcing is 0.10 Sv in the iCESM and 0.05 Sv in the UVic model.
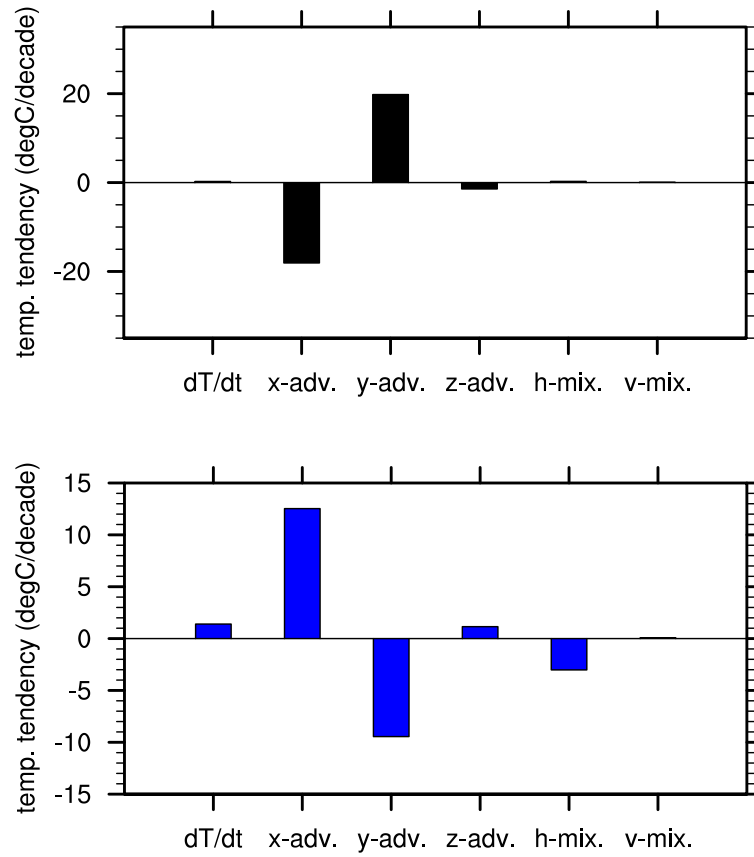
Figure S2. Budget analysis of the subsurface warming. Terms in the temperature equation of the northwestern North Atlantic subsurface ocean (44–46°N, 300–320°E, 400m) in the preindustrial control simulation in iCESM (left; units: °C decade⁻¹). From left to right are: the temperature tendency, the zonal advection, the meridional advection, the vertical advection, the horizontal mixing and vertical mixing. Bottom panel shows the changes averaged between year 91 and 100 in the freshwater perturbation experiments. We note that the subsurface warming is dominantly caused by change in the zonal component of gyre circulations, which is coherent with a reorganization of the subsurface current suggested in Fig 1.
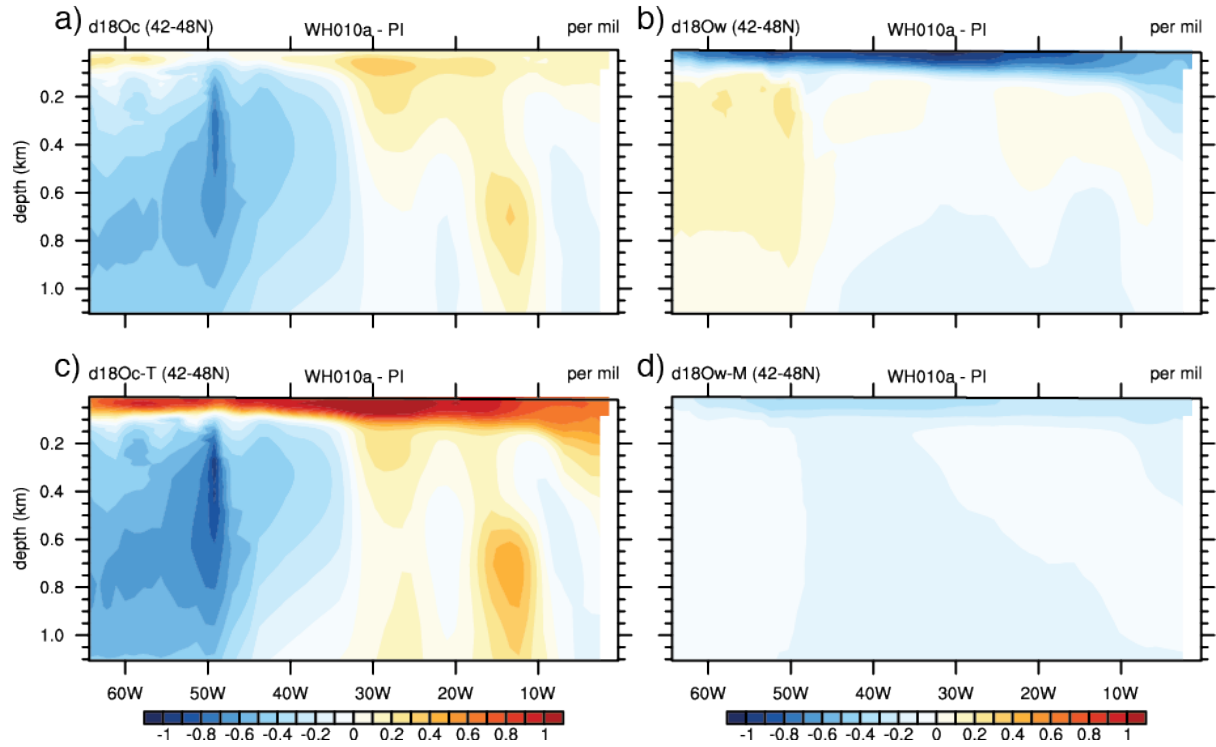
Figure S3. Attributing response of subsurface carbonate δ¹⁸O to freshwater forcing in iCESM. a) Total changes in carbonate δ¹⁸O (units: ‰ PDB) along 45°N in the North Atlantic calculated from modeled changes in seawater δ¹⁸O (units: ‰ SMOW) and ocean temperature using the equation of Shackleton (1974), and contributions from **b)** changes in seawater δ¹⁸O and **c)** ocean temperature. **d)** changes in seawater δ¹⁸O (units: ‰ SMOW) coming from the direct meltwater effect, that is the direct depletion from the depleted freshwater forcing without changes in circulations.
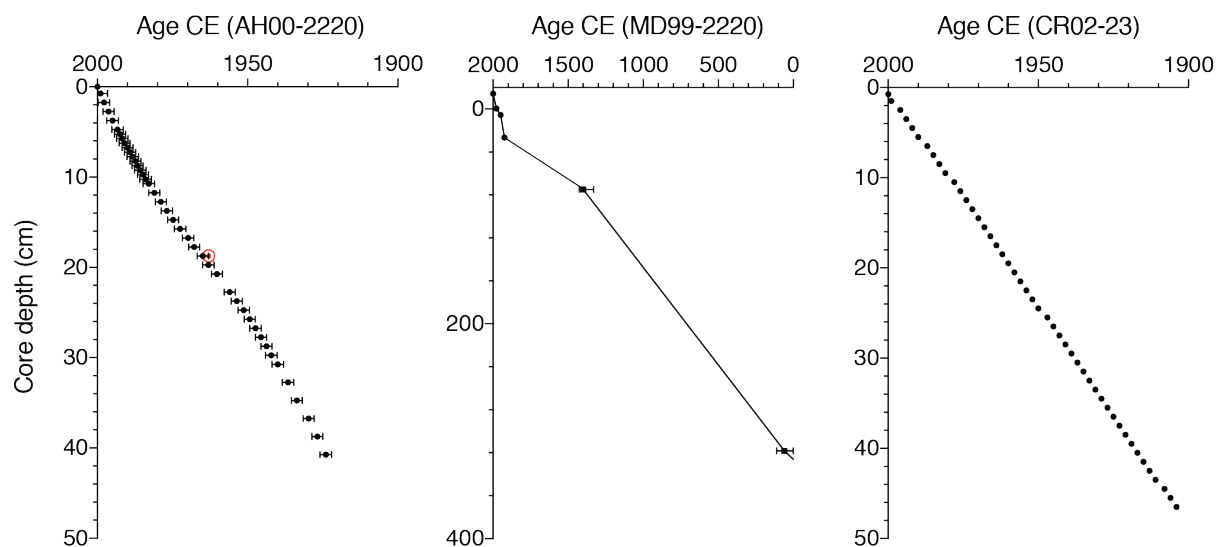
Figure S4. Updated age models for core piston core MD99-2220 and its box core AH00-2220 and box core CR02-23. We updated the ^{210}Pb-derived age model for box cores AH00-2220 and CR02-23 by using the constant rate supply model (Ghaleb, 2009; Sanchez-Cabeza & Ruiz-Fernández, 2012), which estimate the age of each layer independently (i.e., the sedimentation rate can vary in this model). Previous models have used a constant initial concentration model, which implies a constant sedimentation rate. The precision (±1.8 years) of the ^{210}Pb-derived age model for box core AH00-2220 was determined by comparing the ^{210}Pb-derived age to the highest concentration of ^{137}Cs (1964.8), which is attributed to the peak (red dot) of nuclear testing in 1963 (Left panel). The middle panel shows the composite age model for piston core MD99-2220, which lost its top 14 cm in the coring process. The right panel represents the ^{210}Pb-derived age model for box core CR02-23. Detailed data and calculation for the age models are available in the online data.
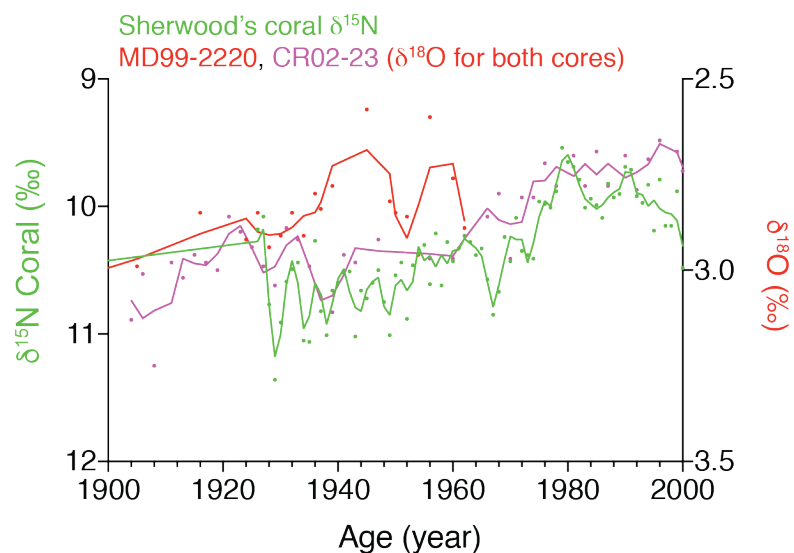
Figure S5. $\delta^{18}O$ from core MD99-2220 (red) and CR02-23 (pink) and $\delta^{15}N$ from Sherwood's corals. The $\delta^{18}O$ at 1900 is 3‰ for MD99-2220 and 3.10‰ for CR02-23. The lowest value is 2.6‰ for MD and 2.66‰ for CR. Thus, the amplitude of the change is similar. There is a clear offset between the dating of the lowest value, which happen much faster in core MD. Since we know the top of the core was lost during the piston coring of MD, we rather not used this part of the core and focus our high-resolution analysis on the box core CR that is well dated with [210]Pb
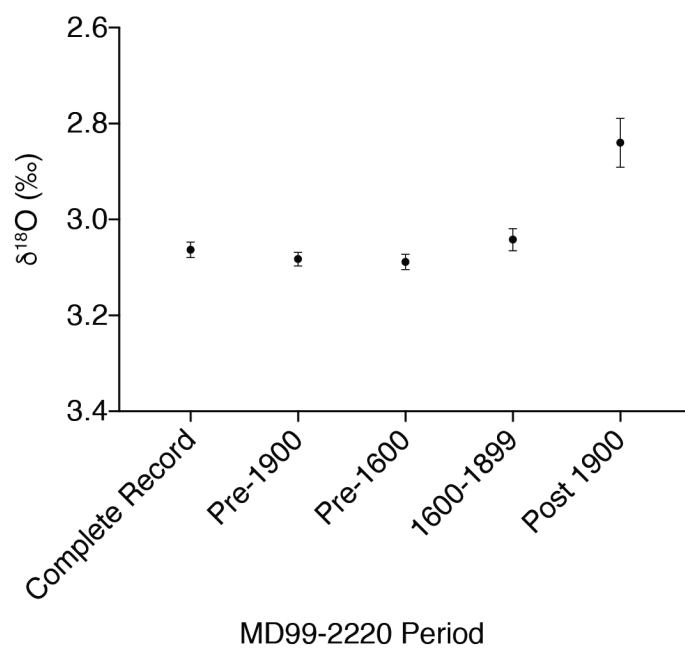
Figure S6. Means and confidence intervals (95%) of the different time periods in core MD99-2220. The post-1900 period is significantly different than any other period while the 1600-1899 period is significantly different than the pre-1600 period.